Vector Soliton Fission

F. Lu, Q. Lin, W. H. Knox, and Govind P. Agrawal
Institute of Optics, University of Rochester, Rochester, NY 14627, USA
(Received 18 March 2004; published 28 October 2004)

We investigate the vectorial nature of soliton fission in an isotropic nonlinear medium both theoretically and experimentally. As a specific example, we show that supercontinuum generation in a tapered fiber is extremely sensitive to the input state of polarization. Multiple vector solitons generated through soliton fission exhibit different states of elliptical polarization while emitting nonsolitonic radiation with complicated polarization features. Experiments performed with a tapered fiber agree with our theoretical description.

DOI: 10.1103/PhysRevLett.93.183901 PACS numbers: 42.81.Dp, 42.65.Re, 42.81.Gs

Solitons represent a fascinating manifestation of the nonlinear phenomena in nature and occur in many branches of physics [1–3]. In the context of optics, solitons forming inside optical fibers have attracted the most attention [4]. It was discovered during the 1980s that higher-order optical solitons undergo *fission* when input pulses exciting them were relatively short [5]. This fission process has become relevant in recent years with the advent of new types of fibers, such as photonic-crystal fibers (PCF) and tapered fibers, because of their unique nonlinear and dispersive properties [6]. Femtosecond optical pulses propagating inside such fibers can generate *supercontinuum* (SC), spanning a broad spectral region from violet to infrared, even when the spectrum of input pulses is only a few nanometers wide [7,8]. The underlying physical mechanism behind SC generation in the anomalous-dispersion regime is believed to be associated with the fission of higher-order solitons [9].

Although SC generated inside birefringent PCF exhibits polarization-dependent features [10–12], soliton-fission process in nearly isotropic fibers has so far been modeled using a scalar nonlinear Schrödinger (NLS) equation [9]. Nonlinear effects in optical fibers are known to be highly polarization-dependent [5]. For this reason, we expect the soliton-fission process to be sensitive to pulse polarization even in an *isotropic* fiber. Indeed, the polarization issues were first studied in 1974 in the context of collisions of two vector solitons [13]. In this Letter, we study, both theoretically and experimentally, SC generation inside isotropic tapered fibers and show that the vectorial nature of soliton fission is important and affects the SC even in the absence of fiber birefringence. Our results show that the fission of a higher-order soliton generates multiple vector solitons that are polarized elliptically along well-defined directions on the Poincaré sphere.

The propagation of ultrashort pulses inside an isotropic optical fiber is governed by the following generalized NLS equation [14]:

$$\frac{\partial \mathbf{A}}{\partial z} = \sum_{m=2}^{7} i^{m+1} \frac{\beta_m}{m!} \frac{\partial^m \mathbf{A}}{\partial \tau^m} + i\gamma\left(1 + \frac{i}{\omega_0}\frac{\partial}{\partial \tau}\right)\mathbf{P}^{(3)}, \quad (1)$$

where β_m is the mth-order dispersion parameter at the carrier frequency ω_0. The nonlinear parameter $\gamma = n_2\omega_0/(ca_{\text{eff}})$, where $n_2 \approx 3 \times 10^{-20}$ m^2/W for silica fibers and the effective core area a_{eff} is ~ 3 μm^2 at 920 nm. The Jones vector $\mathbf{A}$ is a column vector in a linear polarization base. The third-order nonlinear polarization $\mathbf{P}^{(3)}(z, \tau)$ includes both the instantaneous electronic response and delayed Raman response. For silica glass, it has the form [14,15]

$$\mathbf{P}^{(3)} = (1 - f_R)\left\{\frac{2}{3}[\mathbf{A}^*(z, \tau) \cdot \mathbf{A}(z, \tau)]\mathbf{A}(z, \tau) + \frac{1}{3}[\mathbf{A}(z, \tau) \cdot \mathbf{A}(z, \tau)]\mathbf{A}^*(z, \tau)\right\} + f_R\mathbf{A}(z, \tau) \times \int_{-\infty}^{\tau} d\tau' h_R(\tau - \tau')\mathbf{A}^*(z, \tau') \cdot \mathbf{A}(z, \tau'), \quad (2)$$

where $f_R = 0.18$ represents the fractional contribution of nuclear motion. The Raman response is taken to be $h_R(\tau) = [(\tau_1^2 + \tau_2^2)/(\tau_1\tau_2^2)]\exp(-\tau/\tau_2)\sin(\tau/\tau_1)$, where $\tau_1 = 12.2$ fs and $\tau_2 = 32$ fs [5].

Our numeric simulations are performed using parameter values appropriate for the tapered fiber used in the experiment. We estimate $\beta_2 = -24.18$ps^2/km and $\gamma = 44.8$ W^{-1}/km; other dispersion parameters were calculated using a known technique [8]. We solve Eq. (1) numerically with the split-step Fourier method [5] for an almost linearly polarized input "sech" pulse. More specifically, we use $\mathbf{A}(0, \tau) = \sqrt{P_0}\text{sech}(\tau/\tau_0)(\cos\theta, i\sin\theta)$, where the ellipticity angle $\theta = 1.43°$ corresponds to $<0.1\%$ of the input power into the y-polarized component of the pulse. For a peak power $P_0 = 10$ kW and a pulse width $\tau_0 = 85$ fs (FWHM = 150 fs), the input pulse excites a soliton whose order is $N = (\gamma P_0\tau_0^2/|\beta_2|)^{1/2} \approx 12$.

Figure 1 shows the temporal and spectral evolution of the pulse at three propagation distances. During the initial

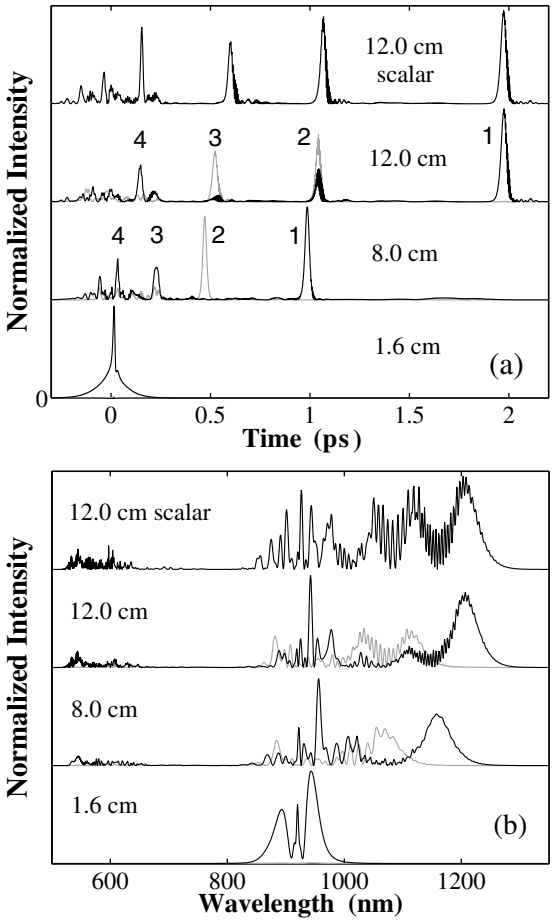

FIG. 1. Numerically simulated temporal (a) and spectral (b) patterns at a distance of 1.6, 8, and 12 cm when a 150-fs pulse is launched into a tapered fiber. The black and gray curves show the two linearly polarized components, respectively. The scalar case at $z = 12$ cm is also shown for comparison.

stage of pulse compression, the pulse remains almost linearly polarized, and no splitting occurs until $z = 1.6$ cm. Beyond that distance, the higher-order soliton undergoes fission and breaks into multiple fundamental vector solitons with different states of polarization (SOPs). The SOP of the rightmost soliton in Fig. 1(a) is close to linear, but others are elliptically polarized. For example, the second soliton has an ellipticity angle of 5.4°, but the third one has an ellipticity angle of 15.4°. The fourth soliton has an ellipticity angle of 16°, and its SOP rotates in a direction opposite to the second and third solitons. The temporal structure near $\tau = 0$ contains the remaining pulse energy and exhibits even more complex polarization features. Successive solitons emerge from this structure. In general, the later the vector soliton is created, the more complicated is its polarization behavior. A comparison of the scalar and vector traces at a distance of 12 cm shows that the vectorial nature of the fission affects the delay experienced by individual solitons.

The spectra shown in Fig. 1(b) reveal the details of SC generation in a tapered fiber. After the fission of the higher-order soliton, all individual solitons experience a large frequency downshift and time delay because of intrapulse Raman scattering [5,16]. The soliton created the earliest is delayed the most because it undergoes the most redshift. As the spectra of these solitons overlap, they interfere with each other and produce the fine oscillatory structure seen in Fig. 1(b). However, since the orthogonally polarized components do not interfere with each other, the magnitude of such oscillations varies dramatically with distance. The spectrum at 12 cm is quite different from that predicted by the scalar NLS equation, indicating that the vectorial effects must be included even when the fiber has almost no birefringence.

The important question is why the SOP of the input pulse changes so drastically in an isotropic nonlinear medium. The answer is provided by the fact that as long as the y component of the field is not zero, the two polarization components are coupled nonlinearly. More precisely, self-phase modulation (SPM), cross-phase modulation (XPM), and other higher-order nonlinear effects such as self-steepening and stimulated Raman scattering induce energy transfer between them. Under conditions appropriate for SC generation, the combined effects of SPM and higher-order dispersion dramatically amplify the energy transfer and split the input pulse into multiple parts interacting with each other through XPM. Such interactions induce drastic polarization variations as the input pulse evolves into individual solitons and dispersive waves.

To gain more physical insight, we introduce a time-dependent Stokes vector $\hat{S}(z, \tau)$, whose tip moves on the Poincaré sphere with north pole as the left circular polarization [17]. Figure 2 depicts the motion of $\hat{S}$ on this sphere under four different conditions. Figure 2(a) shows $\hat{S}$ across the pulse at $z = 1.6$ cm. Since the input pulse is almost linearly polarized, SPM rotates the Stokes vector around the vertical axis [5]. Different parts of the pulse acquire slightly different SOPs but all parts remain nearly linearly polarized. As the compressed pulse is highly chirped, such temporal SOP variations are associated with different frequency components and are responsible for the vectorial nature of the fission process.

After 1.6 cm, higher-order dispersive effects keep moving the upshifted and downshifted frequency components of the pulse toward its tailing edge and initiate the fission process. The compressed pulse splits into multiple components that develop different SOPs through the intense interactions between nonlinearity and dispersion. Various temporal components of the pulse with different SOPs collide with one another as they evolve into individual solitons and generate dispersive waves, as seen in Fig. 1(a). The soliton that is created first (at a distance of about 2 cm in our case) has nearly the same polarization as the input pulse because such collisions do not last long enough to induce large polarization variations. Solitons created further down the fiber acquire elliptical

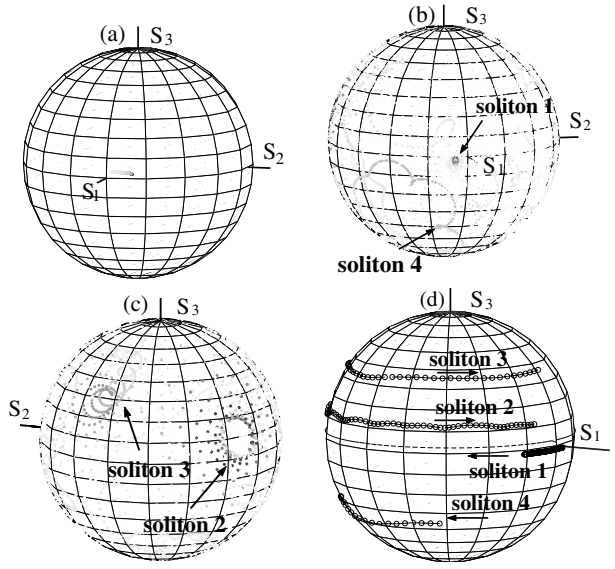

FIG. 2. Polarization patterns in four different cases; grayness of dots indicates intensity. (a) Temporal pattern at $z = 1.6$ cm; (b) temporal pattern at $z = 12$ cm; (c) back of the Poincaré sphere at $z = 12$ cm; (d) z-dependent polarization evolution of four vector solitons.

SOPs since their interactions with other temporal components last longer and hence can induce considerable polarization rotation on individual solitons. Generally speaking, the ellipticity of a vector soliton created through fission depends on the time it is perturbed by the induced nonlinear polarization rotation; the earlier the soliton is formed, the less its SOP changes.

Figs. 2(b) and 2(c) show the front and the back of the Poincaré sphere on which we depict the SOPs of the entire temporal pattern created at a distance of 12 cm (see Fig. 1). Once a vector soliton is formed, its SOP is no longer affected by XPM since its two orthogonally polarized components are bound together and form a pair (the so-called soliton trapping). However, its SOP still evolves in a periodic fashion along the fiber because of SPM. This periodic evolution is shown in Fig. 2(d) for the four solitons up to a distance of 20 cm. The Stokes vector, averaged over the soliton profile, rotates around the vertical axis for each soliton. Note that Fig. 2(d) shows SOP changes as function of distance in contrast with the other three parts of Fig. 2 where SOP varies with time at a fixed distance. Several other features of Fig. 2(d) are noteworthy. As explained earlier, the SOP of the first soliton changes little and it remains almost linearly polarized. The second and third solitons rotate their SOPs counterclockwise, whereas those of the first and fourth solitons rotate clockwise. The rotation rates are also different for all solitons. For example, the second soliton changes polarization in a periodic fashion with a 19.8-cm period but the third one with a period of about 10.4 cm.

An interesting feature seen in Figs. 2(b) and 2(c) is that the SOP of nonsoliton radiation, or dispersive waves (light gray dots), is spread over the entire Poincaré sphere. Physically, as solitons are perturbed by higher-order dispersive and nonlinear effects, they shed part of their energy in the form of dispersive waves. Frequencies of these waves are often shifted toward the blue side, as seen in Fig. 1(b), because of a phase-matching condition related to four-wave mixing. The SOP of a dispersive-wave is set by the SOP of the soliton at the time the radiation is emitted. Since SOPs of the solitons are not fixed but evolve with distance, the SOPs of dispersive waves eventually spread over the entire Poincaré sphere. In the spectral domain, dispersive waves show quite complicated polarization characteristics since each spectral component may get its power from several different solitons. However, because of the phase-matching condition, a soliton with the most redshift generates dispersive waves with the most blueshift and correlates in their polarizations.

Our numerical simulations show that the vectorial fission process is very sensitive to the parameters associated with the input pulse and the fiber. For example, even a slight increase in the relative intensity of the y component at the input end (-30 dB in place of -32 dB) changes the situation enough that even the first soliton in Fig. 1 becomes elliptically polarized. On the other hand, vectorial nature of the soliton fission persists numerically even when the relative intensity level of the y component is down to -50 dB. A commercial mode-locked laser typically contains more power in the orthogonally polarized component than that, indicating that such polarization effects should be observable experimentally. As realistic fibers inevitably exhibit some birefringence, we have included its effects in our numerical simulations using an index difference of $\delta n = 10^{-8}$ for the two polarization components. We find that the results and our conclusions do not change as long as the beat length is much longer than the fiber length used for SC generation.

Our experiments are performed using a tapered fiber which has a 17-cm-long waist with 2.7 μm diameter, two 2-cm-long transition regions, and the head and tail sections of 10 cm [18]. As the fiber is carefully tapered, its birefringence is expected to be small ($\delta n \sim 10^{-8}$). We verified that this indeed was the case by sending a linearly polarized low-power beam into the fiber and varying the input polarization angle. Mode-locked pulses of 100-fs width, generated from a Ti:sapphire laser (Mai Tai) operating at 920 nm at a repetition rate of 80 MHz with an average power of 300 mW, are coupled into the fiber and the generated SC spectrum is recorded with a resolution of 10 nm using an optical spectrum analyzer. In contrast with the case of birefringent PCF [10–12], we did not observe any significant change in the recorded spectrum while rotating the input polarization angle; this feature verifies that our fiber has negligible birefringence.

To analyze the polarization properties of the SC, we inserted a frequency-independent polarizer at the output

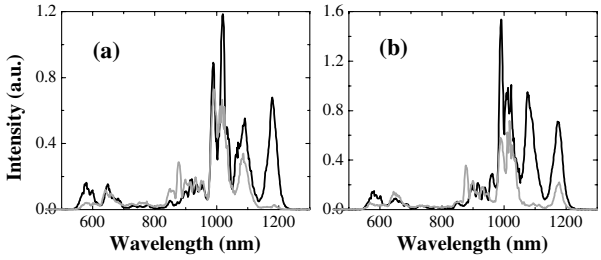

FIG. 3. Experimental SC spectra obtained by rotating a polarizer placed at the output end of the tapered fiber. The black and gray curves show orthogonally polarized components. Polarization contrast is maximized (a) for the rightmost spectral peak and (b) for the peak before that.

end. Figure 3(a) shows the spectra for orthogonal polarizations when the polarizer was oriented to maximize the contrast between the two components for the rightmost spectral peak located at 1180 nm. We recorded a series of such spectra to average the experimental data reported below. We found that the first soliton is elliptically polarized, and the polarization ellipse is oriented at about 3° with respect to the input. The 17.9-dB contrast (average value) for this peak corresponds to an ellipticity angle of $\theta = 7.3° \pm 1.5°$. Notice that the polarization properties of this soliton correlate well with the most blue-shifted dispersive-wave component near 580 nm, as expected from our theory. Figure 3(b) shows the cases in which polarizer is oriented to provide maximum contrast of 15.5 dB for the second spectral peak at 1080 nm. The ellipticity angle is $9.5° \pm 2°$ for this soliton, and its principal axes are oriented at 30° with respect to the input. Other spectral peaks at 990 nm and 1020 nm are even more elliptically polarized. However, since their spectra overlap considerably, it is difficult to distinguish between them. In general, the closer the peak to the input wavelength, the more complicated and unstable is its polarization behavior. We have performed numerical simulations using parameter values most appropriate to our experiment. We find that the ellipticity angles for the first two solitons are 7.2° and 8.6°, respectively. These numbers agree reasonably well with our data within experimental errors. Some discrepancy may also be due to our neglect of the slight anisotropic nature of Raman process. The oscillatory structure seen in Fig. 1(b) does not appear in the experimental spectra because of a relatively low resolution of the optical spectrum analyzer and the averaging induced by its long response time [19–21].

In conclusion, we have shown that the vectorial nature of soliton fission plays an important role in SC generation in weakly birefringent and isotropic fibers. The fission-generated vector solitons are elliptically polarized even when the input pulse is almost linearly polarized. Experiments performed with a tapered fiber agree well with the theory and numerical simulations. Our research suggests that SC generation in weakly birefringent fibers is rarely a scalar process, as often assumed in previous work. The polarization effects discussed here might affect not only the coherence properties of SC [19] but also its characterization through polarization gating [20] or frequency-resolved optical gating [21], both of which are sensitive to the polarization properties of the SC. As a final remark, although we have focused on tapered fibers, our conclusions should hold for soliton fission in any fast-responding medium with Kerr-type nonlinearity.

This research is supported in part by the NYSTAR program and by National Science Foundation under Grants No. ECS-0320816 and No. ECS-0334982.

[1] Y. Yang, *Solitons in Field Theory and Nonlinear Analysis* (Springer, New York, 2001).
[2] L. A. Dickey, *Soliton Equations and Hamiltonian Systems* (World Scientific, New York, 2003).
[3] Y. S. Kivshar and G. P. Agrawal, *Optical Solitons: From Fibers to Photonic Crystals* (Academic, San Diego, 2003).
[4] G. P. Agrawal, *Fiber-Optic Communication Systems* (Wiley, New York, 2002), 3rd ed.
[5] G. P. Agrawal, *Nonlinear Fiber Optics* (Academic, San Diego, 2001), 3rd ed.
[6] P. S. J. Russell, Science **299**, 358 (2003).
[7] J. K. Ranka, R. S. Windeler, and A. J. Stentz, Opt. Lett. **25**, 25 (2000).
[8] T. A. Birks, W. J. Wadsworth, and P. St. J. Russell, Opt. Lett. **25**, 1415 (2000).
[9] A. V. Husakou and J. Herrmann, Phys. Rev. Lett. **87**, 203901 (2001).
[10] A. Apolonski, B. Povazay, A. Unterhuber, W. Drexler, W. J. Wadsworth, J. C. Knight, and P. St. J. Russell, J. Opt. Soc. Am. B **19**, 2165 (2002).
[11] M. Lentonen, G. Genty, and H. Ludvigsen, Appl. Phys. Lett. **82**, 2197 (2003).
[12] Z. Zhu and T. G. Brown, J. Opt. Soc. Am. B **21**, 249 (2004).
[13] S. V. Manakov, Sov. Phys. JETP **38**, 248 (1974).
[14] E. A. Golovchenko and A. N. Pilipetskii, J. Opt. Soc. Am. B **11**, 92 (1994).
[15] R. W. Hellwarth, Prog. Quantum Electron. **5**, 1 (1977).
[16] J. P. Gordon, Opt. Lett. **11**, 662 (1986).
[17] M. Born and E. Wolf, *Principles of Optics* (Cambridge University Press, New York, 1999), 7th ed.
[18] F. Lu and W. H. Knox, Opt. Express **12**, 347 (2004).
[19] J. M. Dudley and S. Coen, Opt. Lett. **27**, 1180 (2002).
[20] H. Kano and H. Hamaguchi, Opt. Lett. **28**, 2360 (2003).
[21] X. Gu, L. Xu, M. Kimmel, E. Zeek, P. O'Shea, A. P. Shreenath, and R. Trebino, Opt. Lett. **27**, 1174 (2002).